Double Negative Metamaterial Sensor Based on Microring Resonator

Jing Jing Yang, Ming Huang, and Jun Sun

***Abstract*—Metamaterials are artificial media structured on a size scale smaller than the wavelength of external stimuli, and may provide novel tools to significantly enhance the sensitivity and resolution of the sensors. In this paper, we derive the dispersion relation of cylindrical dielectric waveguide loaded on double negative metamaterial (DNM) layer, and compute the resonant frequencies and electric field distribution of the corresponding Whispering-Gallery-Modes (WGM). Theoretical results of resonant frequency and electric field distribution are in good agreement with the simulation results. We show that the DNM sensor based on microring resonator possesses higher sensitivity than the traditional microring sensor since the amplification of evanescent wave, and with the increase of metamaterial layer thickness, the sensitivity will be increased greatly. It might open an avenue for designing perfect sensors.**

***Index Terms*—Evanescent wave, metamaterials, microring, sensor.**

I. Introduction

Of PARTICULAR interest, artificially engineered metamaterials are composed of electrically small inclusions that may tailor the material's effective permittivity and permeability with positive, near zero, or negative values. The peculiar properties and often counterintuitive behavior of metamaterials opens possibilities to form various structures with novel functionalities such as perfect lens, cloak, directive antenna, transparent devices, etc. [1]–[5]. Recently, great interest has been devoted to sensing applications of metamaterials. For example, Jakšić *et al.* [6] investigated some peculiarities of electromagnetic metamaterials convenient for plasmon-based chemical sensing with enhanced sensitivity, and they envisioned the practical applications of metamaterial-based sensors in biosensing, chemical sensing, environmental sensing, homeland security, etc. He *et al.* [7], studied the resonant modes of a 2D subwavelength open resonator, and showed it was suitable for biosensing. Cubukcu *et al.* [8] reported a surface enhanced molecular detection technique with zeptomole sensitivity that relies on the resonant electromagnetic coupling between a split ring resonator and the infrared vibrational modes of molecules. Melik *et al.* [9] demonstrated the implementation of metamaterials in wireless RF-MEMS strain sensors, and highly desirable properties were obtained. Alù *et al.* [10] proposed a method of dielectric sensing using ε near-zero narrow waveguide channels. Shreiber [11] developed a novel microwave nondestructive evaluation sensor using metamaterial lens for detection of material defects small relative to a wavelength. Zheludev [12] analyzed the road ahead for metamaterials, and pointed out that sensor applications are another growth area in metamaterials research. Our team [13]–[15] studied the performance of metamaterial sensor, and show that the sensitivity and resolution of the sensors can be greatly enhanced by metamaterials.

WGM is a morphology-dependent resonance. It occurs when light within a dielectric microsphere resonator, which has a higher refractive index than its surrounding. After repeated total internal reflections at the curved boundary, the electromagnetic field can close on itself and give rise to resonances [16]. The WGM resonance phenomenon has attracted increasing attention due to their high potential for the realization of microcavity lasers [17], quantum computers [18], sensing applications [19]–[27], etc. Examples of the applications of WGM sensors include biosensing [22], nanoparticle detection [23], single-molecule detection [24], temperature measurement [25], ammonia detection [26], and TNT detection [27]. However, to the best of our knowledge, there is no report about the DNM sensor based on microring resonator operating in WGM.

The purpose of this paper is to investigate the performance of the DNM sensor and to illustrate how it is different from the traditional microring resonator sensor. First, we derive the dispersion relation of the cylindrical dielectric waveguide loaded on DNM layer, and compute the resonant frequencies and electric field distributions of the corresponding WGMs. Then, we make full wave simulation on the performance of the DNM sensor, and compared with the theoretical results. Finally, we show that the DNM sensor possesses much higher sensitivity than traditional microring resonator sensor, and the mechanism behind these phenomena is verified by theoretical analysis and simulation.

II. Theoretical Analysis

The geometry of cylindrical dielectric waveguide loaded with a layer of metamaterials is shown in Fig. 1. The inner side of the cylindrical dielectric waveguide (ε_3, μ_3) is loaded with a

Manuscript received January 23, 2011; revised February 18, 2011; accepted March 18, 2011. Date of publication March 28, 2011; date of current version August 05, 2011. This work was supported in part by the Training Program of Yunnan Province for Middle-Aged and Young Leaders of Disciplines in Science and Technology under Grant 2008PY031, in part by the Research Foundation from the Ministry of Education of China under Grant 208133, in part by the National Natural Science Foundation of China under Grant 60861002, and in part by NSFC-YN under Grant U1037603. The associate editor coordinating the review of this paper and approving it for publication was Dr. Sandro Carrara.

J. J. Yang and M. Huang are with the School of Information Science and Engineering, Yunnan University, Kunming, Yunnan 650091, China (e-mail: yangjingjing@ynu.edu.cn; huangming@ynu.edu.cn).

J. Sun is with the Faculty of Metallurgical and Energy Engineering, Kunming University of Science and Technology, Kunming 650093, China (e-mail: sunjun_km@yahoo.cn).

Color versions of one or more of the figures in this paper are available online at http://ieeexplore.ieee.org.

Digital Object Identifier 10.1109/JSEN.2011.2132798

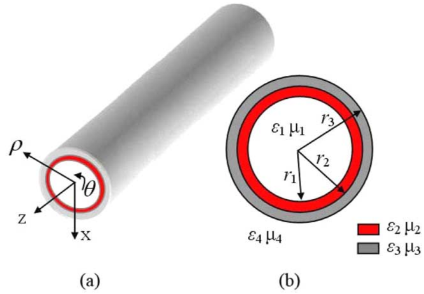

Fig. 1. (Color online) (a) Schematic illustration of the cylindrical dielectric waveguide loaded with a metamaterial layer colored in red. (b) Cross section of the waveguide. $\mu_1 = \mu_3 = \mu_4 = \mu_0, \varepsilon_2 = -\varepsilon_0, \mu_2 = -\mu_0$.

layer of metamaterials (ε_2, μ_2). Material parameters of the inner region and the outer region is denoted as ε_1, μ_1, ε_4, and μ_4. The axial fields in regions 1, 2, 3, and 4 for TM mode [28] are

$$E_z^{(1)}(r,\theta) = A_m J_m(p_1 r)e^{\pm jm\theta} \tag{1a}$$
$$E_z^{(2)}(r,\theta) = (B_m J_m(p_2 r) + B'_m Y_m(p_2 r))\, e^{\pm jm\theta} \tag{1b}$$
$$E_z^{(3)}(r,\theta) = (C_m J_m(p_3 r) + C'_m Y_m(p_3 r))e^{\pm jm\theta} \tag{1c}$$
$$E_z^{(4)}(r,\theta) = D_m K_m(qr)e^{\pm jm\theta} \tag{1d}$$

where A_m, B_m, C_m, D_m, B'_m, and C'_m are chosen here to weight the field but they are interdependent. J_m, Y_m, and K_m are, respectively, the Bessel functions of the first kind, of the second kind, and the modified Bessel function of the second kind. $p_1 = \sqrt{\omega^2\varepsilon_1\mu_1 - \beta^2}$, $p_2 = \sqrt{\omega^2\varepsilon_2\mu_2 - \beta^2}$, $p_3 = \sqrt{\omega^2\varepsilon_3\mu_3 - \beta^2}$, $q = \sqrt{\beta^2 - \omega^2\varepsilon_4\mu_4}$. β is the propagation constant, and m is the angular order. For an infinite cylindrical dielectric waveguide with negligible absorption and no axial component of the propagation constant $(\beta = 0)$, TM mode degenerates to WGM [29], (1) becomes

$$E_z^{(1)}(r,\theta) = A_m J_m(p_1 r)e^{\pm jm\theta} \tag{2a}$$
$$E_z^{(2)}(r,\theta) = (B_m J_m(p_2 r) + B'_m Y_m(p_2 r))\, e^{\pm jm\theta} \tag{2b}$$
$$E_z^{(3)}(r,\theta) = (C_m J_m(p_3 r) + C'_m Y_m(p_3 r))\, e^{\pm jm\theta} \tag{2c}$$
$$E_z^{(4)}(r,\theta) = D'_m H_m^{(1)}(p_4 r)e^{\pm jm\theta} \tag{2d}$$

where $p_1 = \omega\sqrt{\varepsilon_1\mu_1}$, $p_2 = \omega\sqrt{\varepsilon_2\mu_2}$, $p_3 = \omega\sqrt{\varepsilon_3\mu_3}$, $p_4 = \sqrt{-q^2} = \omega\sqrt{\varepsilon_4\mu_4}$, $D'_m = (i\pi/2)e^{im\pi/2}D_m$, $H_m^{(1)}$ is the Hankel function of the first kind. The relation between $H_m^{(1)}$ and K_m is $K_m(-iz) = (i\pi/2)e^{im\pi/2}H_m^{(1)}(\mathrm{z})$. For TM mode in the cylindrical dielectric waveguide, transverse magnetic fields can be obtained as

$$H_r(r,\theta) = \frac{1}{p^2}\left(\frac{j\omega\varepsilon}{r}\frac{\partial E_z(r,\theta)}{\partial\theta}\right) \tag{3a}$$
$$H_\theta(r,\theta) = \frac{1}{p^2}\left(-j\omega\varepsilon\frac{\partial E_z(r,\theta)}{\partial r}\right). \tag{3b}$$

The field matching equations at the boundary surface, $r = r_1$, $r = r_2$, and $r = r_3$ are expressed as

$$E_z^{(1)}(r_1,\theta) = E_z^{(2)}(r_1,\theta), H_\theta^{(1)}(r_1,\theta) = H_\theta^{(2)}(r_1,\theta),$$
$$E_z^{(2)}(r_2,\theta) = E_z^{(3)}(r_2,\theta), H_\theta^{(2)}(r_2,\theta) = H_\theta^{(3)}(r_2,\theta),$$
$$E_z^{(3)}(r_3,\theta) = E_z^{(4)}(r_3,\theta), H_\theta^{(3)}(r_4,\theta) = H_\theta^{(4)}(r_4,\theta).$$

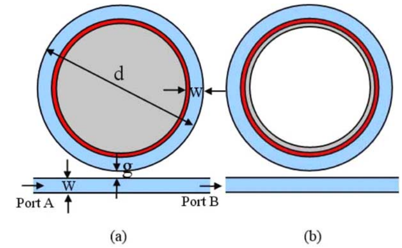

Fig. 2. (Color online) Simulation model. (a) Homogeneous sensing. (b) Surface sensing.

Satisfying these conditions gives

$$[M]\,[A_m, B_m, B'_m, C_m, C'_m, D'_m]^T = 0 \tag{4}$$

where equations (5)–(10) are shown at the bottom of the next page.

The dispersion equation can be obtained by setting $|M| = 0$. Coefficients B_m, B'_m, C_m, C'_m, and D'_m can be expressed in terms of the arbitrary coefficient A_m, which can be determined from the excitation condition, and $B_m = f_m^{(1)}A_m$, $B'_m = f_m^{(2)}A_m$, $C_m = f_m^{(3)}A_m$, $C'_m = f_m^{(4)}A_m$, $D'_m = f_m^{(5)}A_m$. The coefficients $f_n^{(1)}$, $f_n^{(2)}$, $f_n^{(3)}$, $f_n^{(4)}$, and $f_n^{(5)}$ may be found from (4).

III. Results and Discussions

A. Simulation Model

Simulation models of the DNM sensor are shown in Fig. 2. A layer of metamaterials with thickness t is located in the inner side of the microring. Permittivity and permeability of the metamaterials are $\varepsilon_2 = -\varepsilon_0$, $\mu_2 = -\mu_0$. Width of the microring and the waveguide is $w = 0.3\ \mu\mathrm{m}$. The outer diameter of the microring is $d = 5\ \mu\mathrm{m}$. The distance from outer microring to the waveguide is $g = 0.232\ \mu\mathrm{m}$. The permittivity of the microring and the waveguide is $\varepsilon_3 = 10.24\varepsilon_0$. Fig. 2(a) is the simulation model for homogeneous sensing. The dielectric core with permittivity $\varepsilon_1 = \varepsilon_r\varepsilon_0$ is colored in gray. Fig. 2(b) is the simulation model for surface sensing. The dielectric substance with thickness t_s and permittivity $\varepsilon_1 = \varepsilon_r\varepsilon_0$ is attached to the metamaterial layer.

B. Results and Discussions

Frequency spectrum of the DNM sensor for homogeneous sensing is simulated by the commercial software COMSOL multiphysics, as shown in Fig. 3. It is obtained by frequency sweep. The sinusoidal excitation with amplitude of 1 V/m is set at port A of the waveguide. A probe is located at the point that possesses maximum electric filed at resonant state to record variation of $|E_z|$ with frequency. From left to right, the spectral lines represent mode 25, 26, 27, 28, and 29 of the DNM sensor. The inset shows the amplification in the frequency range of 198.68–198.72 THz. A comparison of the analytical and simulated resonant frequency for the microring resonator sensor and the DNM sensor is shown in Table I. It is seen that the

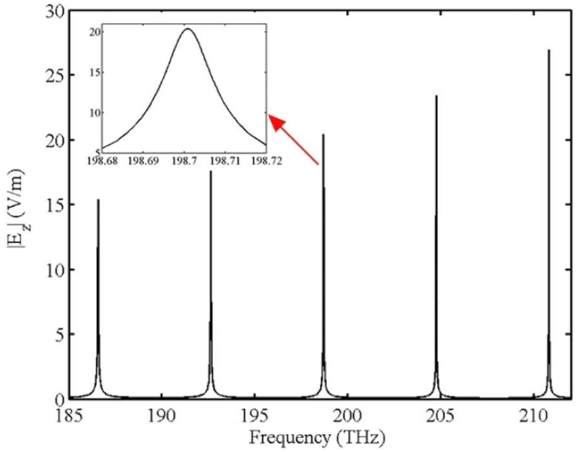

Fig. 3. Frequency spectrum of the DNM sensor. Thickness of the metamaterial layer is $t = 0.12\ \mu\mathrm{m}$. Permittivity of the dielectric core is $\varepsilon_r = 1$.

theoretical results are in good agreement with the simulation results.

TABLE I
COMPARISON OF THE THEORETICAL RESONANT FREQUENCY (f_t THz) AND SIMULATED RESONANT FREQUENCY (f_s THz) FOR THE MICRORING RESONATOR SENSOR AND THE DNM SENSOR

Mode(m)	*25*	*26*	*27*	*28*	*29*
f_t (t=0)	186.145	192.199	198.251	204.300	210.347
f_s (t=0)	186.156	192.208	198.257	204.304	210.351
f_t (t=0.12μm)	186.564	192.630	198.693	204.754	210.815
f_s(t=0.12μm)	186.577	192.640	198.701	204.761	210.821

Taking mode 27 as an example, electric field distribution of the microring sensor and the DNM senor is simulated and compared with that of the analytical results, as shown in Fig. 4. The theoretical electric field distribution is obtained by substituting (6)–(10) in to (2). The simulating results agree quite well with the analytical results. From Fig. 4(a) and (b), we can observe that the maximum electric field is distributed inside the ring for the microring resonator sensor without the metamaterial layer. For the DNM sensor, maximum electric field permeates into the surface of the metamaterial layer, as shown in

$$[M] = \begin{bmatrix} J_m(p_1r_1) & -J_m(p_2r_1) & -Y_m(p_2r_1) & 0 & 0 & 0 \\ -\frac{\varepsilon_1 J'_m(p_1r_1)}{p_1} & \frac{\varepsilon_2 J'_m(p_2r_1)}{p_2} & \frac{\varepsilon_2 Y'_m(p_2r_1)}{p_2} & 0 & 0 & 0 \\ 0 & J_m(p_2r_2) & Y_m(p_2r_2) & -J_m(p_3r_2) & -Y_m(p_3r_2) & 0 \\ 0 & -\frac{\varepsilon_2 J'_m(p_2r_2)}{p_2} & -\frac{\varepsilon_2 Y'_m(p_2r_2)}{p_2} & \frac{\varepsilon_3 J'_m(p_3r_2)}{p_3} & \frac{\varepsilon_3 Y'_m(p_3r_2)}{p_3} & 0 \\ 0 & 0 & 0 & J_m(p_3r_3) & Y_m(p_3r_3) & -H_m^{(1)}(p_4r_3) \\ 0 & 0 & 0 & -\frac{\varepsilon_3 J'_m(p_3r_3)}{p_3} & -\frac{\varepsilon_3 Y'_m(p_3r_3)}{p_3} & \frac{\varepsilon_4 H'^{(1)}_m(p_4r_3)}{p_4} \end{bmatrix} \tag{5}$$

$$f_m^{(1)} = \frac{(p_2\varepsilon_1 J'_m(p_1r_1)Y_m(p_2r_1) - p_1\varepsilon_2 J_m(p_1r_1)Y'_m(p_2r_1))}{(p_1\varepsilon_2 J'_m(p_2r_1)Y_m(p_2r_1) - p_1\varepsilon_2 J_m(p_2r_1)Y'_m(p_2r_1))} \tag{6}$$

$$f_m^{(2)} = \frac{-(p_2\varepsilon_1 J'_m(p_1r_1)J_m(p_2r_1) - p_1\varepsilon_2 J_m(p_1r_1)J'_m(p_2r_1))}{(p_1\varepsilon_2 J'_m(p_2r_1)Y_m(p_2r_1) - p_1\varepsilon_2 J_m(p_2r_1)Y'_m(p_2r_1))} \tag{7}$$

$$f_m^{(3)} = \frac{\begin{array}{l}(p_2\varepsilon_3 Y'_m(p_3r_2)(J_m(p_2r_2)(p_1\varepsilon_2 J_m(p_1r_1)Y'_m(p_2r_1) - p_2\varepsilon_1 J'_m(p_1r_1)Y_m(p_2r_1)) + Y_m(p_2r_2)(p_2\varepsilon_1 J'_m(p_1r_1)J_m(p_2r_1) \\ \quad -p_1\varepsilon_2 J_m(p_1r_1)J'_m(p_2r_1))) + p_3\varepsilon_2 Y_m(p_3r_2)(J'_m(p_2r_2)(p_2\varepsilon_1 J'_m(p_1r_1)\cdot Y_m(p_2r_1) - p_1\varepsilon_2 J_m(p_1r_1)Y'_m(p_2r_1)) \\ \quad +Y'_m(p_2r_2)\cdot(p_1\varepsilon_2 J_m(p_1r_1)J'_m(p_2r_1) - p_2\varepsilon_1 J'_m(p_1r_1)J_m(p_2r_1))))\end{array}}{(p_1p_2\varepsilon_2\varepsilon_3(J'_m(p_2r_1)Y_m(p_2r_1) - J_m(p_2r_1)Y'_m(p_2r_1))(J'_m(p_3r_2)\cdot Y_m(p_3r_2) - J_m(p_3r_2)Y'_m(p_3r_2)))} \tag{8}$$

$$f_m^{(4)} = \frac{\begin{array}{l}(p_2\varepsilon_3 J'_m(p_3r_2)(J_m(p_2r_2)(p_2\varepsilon_1 J'_m(p_1r_1)Y_m(p_2r_1) - p_1\varepsilon_2 J_m(p_1r_1)Y'_m(p_2r_1)) + Y_m(p_2r_2)(p_1\varepsilon_2 J_m(p_1r_1)J'_m(p_2r_1) \\ \quad -p_2\varepsilon_1 J'_m(p_1r_1)J_m(p_2r_1))) + p_3\varepsilon_2 J_m(p_3r_2)(J'_m(p_2r_2)(p_1\varepsilon_2 J_m(p_1r_1)\cdot Y'_m(p_2r_1) - p_2\varepsilon_1 J'_m(p_1r_1)Y_m(p_2r_1)) \\ \quad +Y'_m(p_2r_2)\cdot(p_2\varepsilon_1 J'_m(p_1r_1)J_m(p_2r_1) - p_1\varepsilon_2 J_m(p_1r_1)J'_m(p_2r_1))))\end{array}}{(p_1p_2\varepsilon_2\varepsilon_3(J'_m(p_2r_1)Y_m(p_2r_1) - J_m(p_2r_1)Y'_m(p_2r_1))(J'_m(p_3r_2)\cdot Y_m(p_3r_2) - J_m(p_3r_2)Y'_m(p_3r_2)))} \tag{9}$$

$$f_m^{(5)} = \frac{\begin{array}{l}c_1(Y_m(p_3r_3)(p_2\varepsilon_3 J'_m(p_3r_2)(J_m(p_2r_2)(p_2\varepsilon_1 J'_m(p_1r_1)Y_m(p_2r_1) - p_1\varepsilon_2 J_m(p_1r_1)Y'_m(p_2r_1)) \\ \quad +Y_m(p_2r_2)(p_1\varepsilon_2 J_m(p_1r_1)J'_m(p_2r_1) - p_2\varepsilon_1 J'_m(p_1r_1)J_m(p_2r_1))) \\ \quad +p_3\varepsilon_2 J_m(p_3r_2)(J'_m(p_2r_2)(p_1\varepsilon_2 J_m(p_1r_1)Y'_m(p_2r_1) - p_2\varepsilon_1 J'_m(p_1r_1)Y_m(p_2r_1)) \\ \quad +Y'_m(p_2r_2)(p_2\varepsilon_1 J'_m(p_1r_1)\cdot J_m(p_2r_1) - p_1\varepsilon_2 J_m(p_1r_1)J'_m(p_2r_1)))) \\ \quad +J_m(p_3r_3)(p_2\varepsilon_3 Y'_m(p_3r_2)(J_m(p_2r_2)(p_1\varepsilon_2 J_m(p_1r_1)Y'_m(p_2r_1) \\ \quad -p_2\varepsilon_1 J'_m(p_1r_1)Y_m(p_2r_1)) + Y_m(p_2r_2)(p_2\varepsilon_1 J'_m(p_1r_1)J_m(p_2r_1) \\ \quad -p_1\varepsilon_2 J_m(p_1r_1)J'_m(p_2r_1))) + p_3\varepsilon_2 Y_m(p_3r_2)(J'_m(p_2r_2)(p_2\varepsilon_1 J'_m(p_1r_1)Y_m(p_2r_1) \\ \quad -p_1\varepsilon_2 J_m(p_1r_1)\cdot Y'_m(p_2r_1)) + Y'_m(p_2r_2)(p_1\varepsilon_2 J_m(p_1r_1)J'_m(p_2r_1) \\ \quad -p_2\varepsilon_1 J'_m(p_1r_1)J_m(p_2r_1)))))\end{array}}{(p_1p_2\varepsilon_2\varepsilon_3 H_m^{(1)}(p_4r_3)(J'_m(p_2r_1)Y_m(p_2r_1) - J_m(p_2r_1)\cdot Y'_m(p_2r_1))(J'_m(p_3r_2)Y_m(p_3r_2) - J_m(p_3r_2)Y'_m(p_3r_2)))}. \tag{10}$$

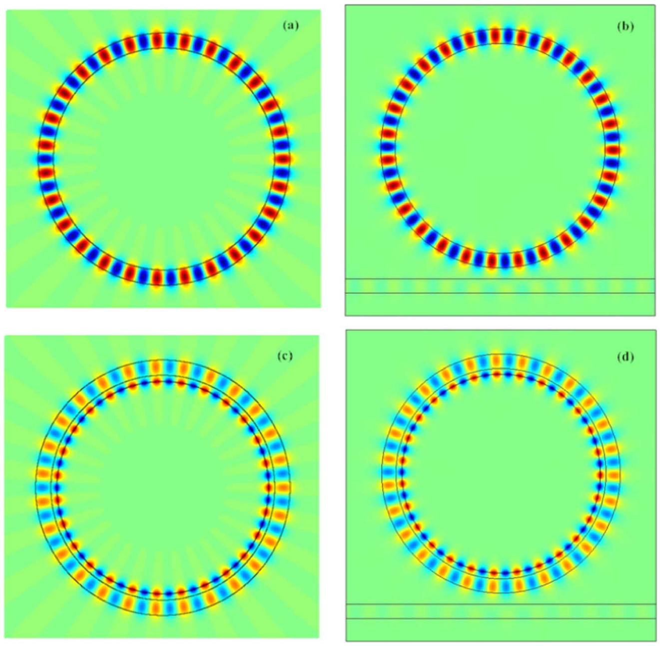

Fig. 4. (Color online) Electric field distribution of the microring sensor operating at mode 27. (a) Theoretical result of the microring resonator sensor. (b) Simulating result of the microring resonator sensor. (c) Theoretical result of the DNM sensor. (d) Simulation result of the DNM sensor. Thickness of the metamaterial layer is $t = 0.12\ \mu\mathrm{m}$.

Fig. 4(c) and (d). Therefore, this area will be quite sensitive in dielectric environment.

Fig. 5 shows the simulating results for homogeneous sensing. Permittivity (ε_r) of the dielectric core varies form 1 to 1.1 with an interval of 0.02. The spectra are red shifted with the increase of (ε_r). From Fig. 5(a) and (b), we can obtain that the average frequency shift for the microring resonator sensor is about 7.562 GHz; for the DNM sensor, the average frequency shift is about 116.137 GHz. Therefore, sensitivity of the DNM sensor is 15.358 times that of the traditional microring resonator sensor for homogeneous sensing.

Resonant frequency in Fig. 5 is calculated and compared with the theoretical method, as shown in Fig. 6. Blue and green lines denote the results for the DNM sensor, obtained by theoretical method and numerical simulation, respectively. Red and cyan lines denote the results for the microring resonator sensor. From Fig. 6, we can observe that the simulation results agree well with the theoretical results. With an increase of 0.02 in core medium permittivity, the average frequency shift of the microring sensor is quite small. When a layer of metamaterials is attached to the inner side of the microring resonator, the average frequency shift of the DNM sensor will be greatly increased. As a consequence, the DNM sensor possesses much higher sensitivity than the traditional microring resonator sensor.

To reveal the mechanism behind these phenomena, we plot the electric field distribution along x axis from -3 to $-1.5\ \mu\mathrm{m}$ for mode 27, as shown in Fig. 7. Permittivity of the core medium is set to be $\varepsilon_r = 1$. It is seen that the electric field intensity increases with metamaterial layer thickness (t). The inset shows the electric filed distribution of the DNM sensor. From Fig. 7, we can clearly observe that the stronger electric field of evanescent wave penetrates into the detecting region when the thickness of metamaterial layer increases. Therefore, the essence for the enhancement of sensitivity is the evanescent wave amplified by metamaterials.

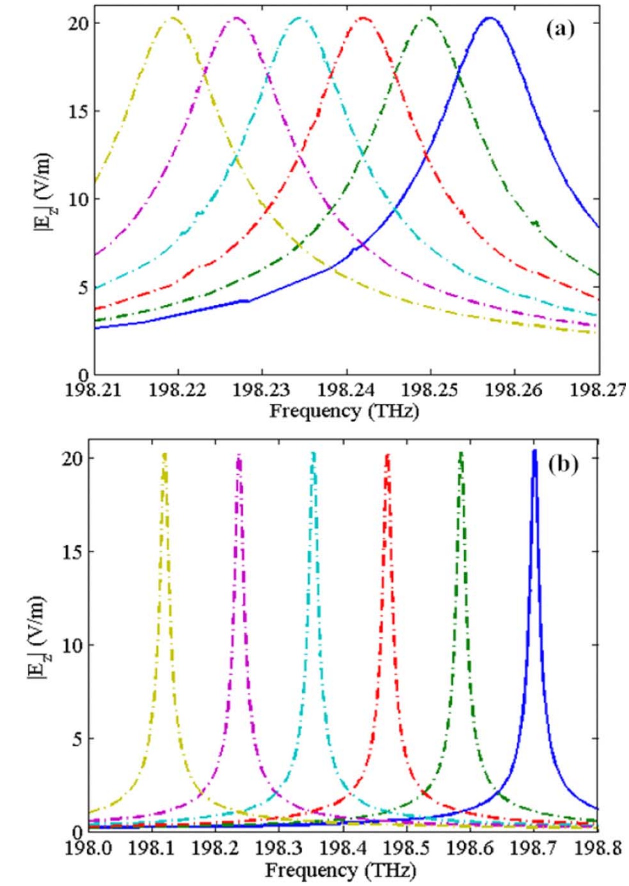

Fig. 5. (Color online) Resonant frequency spectrum of mode 27 with respect to the change of core medium permittivity ε_r. From left to right, the curves correspond to $\varepsilon_r = 1$, 1.02, 1.04, 1.06, 1.08, and 1.1, respectively. (a) The microring resonator sensor. (b) The DNM sensor. Thickness of the metamaterial layer is $t = 0.12\ \mu\mathrm{m}$.

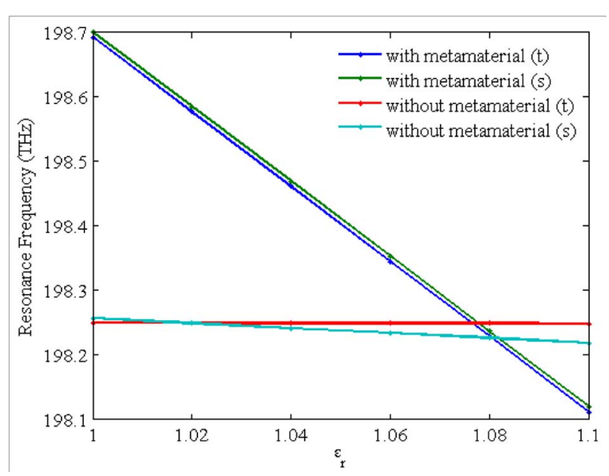

Fig. 6. (Color online) Relation between ε_r and resonant frequency.

Fig. 8 shows the relation between core medium permittivity and resonant frequency for different metamaterial layer thickness. Permittivity of the core medium increases from 1 to 1.1

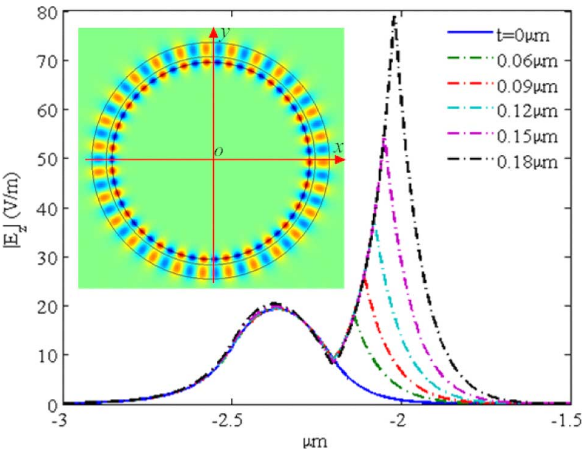

Fig. 7. (Color online) Electric field distribution along x axis from -3 to -1.5 μm for the DNM sensor operating in mode 27. The inset shows the electric field distribution of the DNM sensor, of which the metamaterial layer thickness is $t = 0.12$ μm.

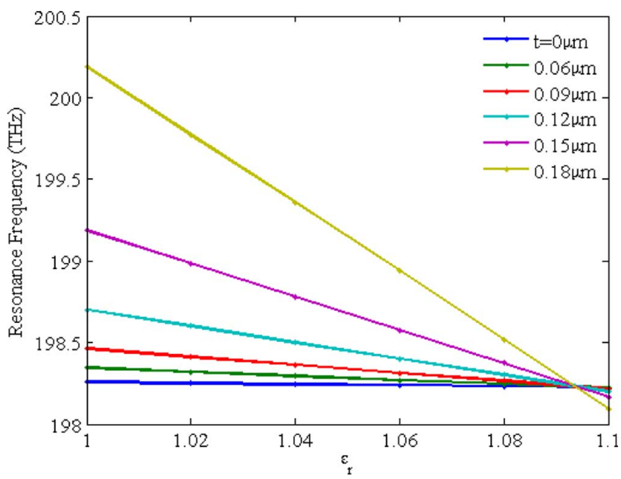

Fig. 8. (Color online) Homogeneous sensing. Relation between ε_r and resonant frequency for a variation of metamaterial layer thickness.

with an interval of 0.02. Resonant frequency shift varies linearly with the permittivity of substance. For the microring resonator sensor, average frequency shift with response to an increase of 0.02 in core medium permittivity is only 7.562 GHz. For the DNM sensor, average frequency shift increases with metamaterial layer thickness. When the thickness of the metamaterial layer is increased to 0.06, 0.09, 0.12, 0.15, and 0.18 μm, the corresponding average frequency shift will be 29.001, 57.744, 116.137, 235.972, and 483.071 GHz, respectively.

Surface sensing of the DNM sensor can also be analyzed according to the above procedures, and it is not shown here for brevity. Fig. 9 portrays the simulation results of surface sensing. Thickness of the adsorbed substance is 0.075 μm. Similarly, average frequency shift increases with metamaterial thickness. When metamaterial layer thickness increases from 0.06 to 0.18 μm with an interval of 0.03 μm, the average frequency shift of the DNM sensor with response to an increase of 0.02 in surface medium permittivity is about 24.525, 49.454, 99.984, 204.167, and 419.610 GHz, respectively. Therefore, sensitivity

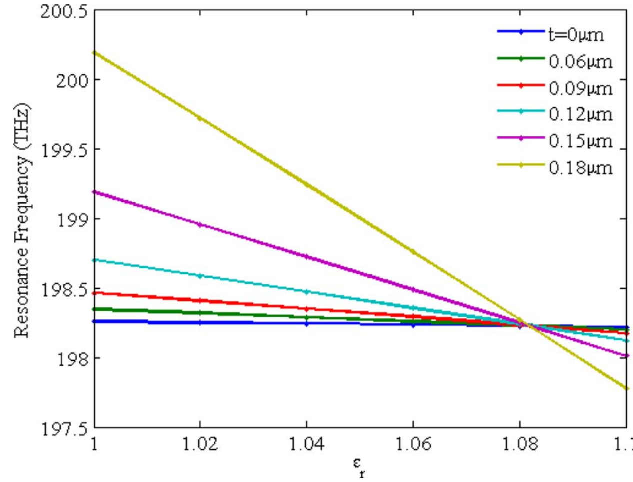

Fig. 9. (Color online) Surface sensing. Relation between ε_r and resonant frequency for a variation of metamaterial layer thickness.

of the DNM sensor can be greatly improved by increasing the thickness of the metamaterial layer attached to its inner side.

IV. Conclusion

WGMs of dielectric waveguide with a layer of metamaterials is theoretically analyzed, and the dispersion relation is derived. Analytical results of the resonant frequency shift and electric field distribution of the sensor is in good agreement with the simulation results. We show that the DNM sensor possesses a higher sensitivity than the traditional microring resonator sensor, since the amplification of evanescent wave. Moreover, the sensitivity will be further improved by increasing the thickness of the metamaterial layer. It opens an avenue for design novel sensors with specified sensitivity.

References

[1] J. B. Pendry, "Negative refraction makes a perfect lens," *Phys. Rev. Lett.*, vol. 85, no. 18, pp. 3966–3969, Oct. 2000.

[2] J. B. Pendry, D. Schurig, and D. R. Smith, "Controlling electromagnetic fields," *Science*, vol. 312, no. 5781, pp. 1780–1782, Jun. 2006.

[3] P. Alitalo and S. Tretyakov, "Electromagnetic cloaking with metamaterials," *Materials Today*, vol. 12, pp. 22–29, Mar. 2009.

[4] W. X. Jiang, J. Y. Chin, and T. J. Cui, "Anisotropic metamaterial devices," *Materials Today*, vol. 12, pp. 26–33, Dec. 2009.

[5] A. E. Dubinov and L. A. Mytareva, "Invisible cloaking of material bodies using the wave flow method," *Physics—Uspekhi*, vol. 53, no. 5, pp. 455–479, May 2010.

[6] Z. Jakšic, Z. Djuric, and C. Kment, "A consideration of the use of metamaterials for sensing applications: Field fluctuations and ultimate performance," *J. Opt. A: Pure Appl. Opt.*, vol. 9, pp. S377–S377, Sep. 2007.

[7] S. He, Y. Jin, Z. C. Ruan, and J. G. Kuang, "On subwavelength and open resonators involving metamaterials of negative refraction index," *New J. Phys.*, vol. 7, no. 1, p. 210, Mar. 2005.

[8] E. Cubukcu, S. Zhang, Y. S. Park, G. Bartal, and X. Zhang, "Split ring resonator sensors for infrared detection of single molecular monolayers," *Appl. Phys. Lett.*, vol. 95, no. 4, pp. 043113–043113, Aug. 2009.

[9] R. Melik, E. Unal, N. K. Perkgoz, C. Puttlitz, and H. V. Demir, "Metamaterial-based wireless strain sensors," *Appl. Phys. Lett.*, vol. 95, no. 4, pp. 011106–011106, Jul. 2009.

[10] A. Alù and N. Engheta, "Dielectric sensing in ε-near-zero narrow waveguide channels," *Phys. Rev. B*, vol. 78, no. 4, pp. 045102–045102, Jul. 2008.

[11] D. Shreiber, M. Gupta, and R. Cravey, "Comparative study of 1-D and 2-D metamaterial lens for microwave nondestructive evaluation of dielectric materials," *Sens. Actuators A: Phys*, vol. 165, no. 2, pp. 256–260, Feb. 2011.
[12] N. I. Zheludev, "The road ahead for metamaterials," *Science*, vol. 328, no. 5978, pp. 582–583, Apr. 2010.
[13] M. Huang, J. J. Yang, J. Sun, J. H. Shi, and J. H. Peng, "Modelling and analysis of Ω-shaped double negative material-assisted microwave sensor," *J. Infrared Milli. Terahz. Waves*, vol. 30, no. 11, pp. 1131–1138, Jul. 2009.
[14] J. J. Yang, M. Huang, Z. Xiao, and J. H. Peng, "Simulation and analysis of asymmetric metamaterial resonator-assisted microwave sensor," *Mod. Phys. Lett. B*, vol. 24, no. 12, pp. 1207–1215, Dec. 2010.
[15] M. Huang and J. J. Yang, *Microwave Sensor Using Metamaterials*, ser. Wave Propagation, A. Petrin, Ed. Vienna, Austria: Intech Press, 2011, ch. 2.
[16] H. Quan and Z. Guo, "Simulation of whispering-gallery-mode resonance shifts for optical miniature biosensors," *J. Quantitative Spectroscopy & Radiative Transfer*, vol. 93, no. 1–3, pp. 231–243, Jun. 2005.
[17] C. Walther, G. Scalari, M. I. Amanti, M. Beck, and J. Faist, "Microcavity laser oscillating in a circuit-based resonator," *Science*, vol. 327, no. 5972, pp. 1495–1497, Mar. 2010.
[18] T. D. Ladd, F. Jelezko, R. Laflamme, Y. Nakamura, C. Monroe, and J. L. O'Brien, "Quantum computers," *Nature*, vol. 464, no. 7285, pp. 45–53, Mar. 2010.
[19] K. J. Vahala, "Optical microcavities," *Nature*, vol. 424, no. 6950, pp. 839–846, Aug. 2003.
[20] D. K. Armani, T. J. Kippenberg, S. M. Spillane, and K. J. Vahala, "Ultra-high-Q toroid microcavity on a chip," *Nature*, vol. 421, no. 6926, pp. 925–928, Feb. 2003.
[21] H. K. Hunt, C. Soteropulos, and A. M. Armani, "Bioconjugation strategies for microtoroidal optical resonators," *Sensors*, vol. 10, no. 10, pp. 9317–9336, Oct. 2010.
[22] F. Vollmer and S. Arnold, "Wispering-gallery-mode biosensing: Label-free detection down to single molecules," *Nature Methods*, vol. 5, no. 7, pp. 591–596, Jun. 2008.
[23] J. Zhu, S. K. Ozdemir, Y. F. Xiao, L. Li, L. He, D. R. Chen, and L. Yang, "On-chip single nanoparticle detection and sizing by mode splitting in an ultrahigh-Q microresonator," *Nature Photonics*, vol. 4, no. 1, pp. 46–49, Jan. 2010.
[24] A. M. Armani, R. P. Kulkarni, S. E. Fraser, R. C. Flagan, and K. J. Vahala, "Label-free, single-molecule detection with optical microcavities," *Science*, vol. 317, no. 5839, pp. 783–787, Aug. 2007.
[25] Q. Ma, T. Rossmann, and Z. Guo, "Whispering-gallery mode silica microsensors for cryogenic to room temperature measurement," *Meas. Sci. Technol.*, vol. 21, no. 2, pp. 025310–025310, Feb. 2010.
[26] V. M. N. Passaro, F. Dell'Olio, and F. De Leonardis, "Ammonia optical sensing by microring resonators," *Sensors*, vol. 7, no. 11, pp. 2741–2749, Nov. 2007.
[27] R. Orghici, P. Lützow, J. Burgmeier, J. Koch, H. Heidrich, W. Schade, N. Welschoff, and S. Waldvogel, "A microring resonator sensor for sensitive detection of 1, 3, 5-Trinitrotoluene (TNT)," *Sensors*, vol. 10, no. 7, pp. 6788–6795, Jul. 2010.
[28] C. Yeh and F. Shimabukuro, *The Essence of Dielectric Waveguides*. New York: Springer, 2008, ch. 5.
[29] J. Heebner, R. Grover, T. Ibrahim, and T. Ibrahim, *Optical Microresonators: Theory, Fabrication, and Applications*. New York: Springer, 2008, ch. 2.

Jingjing Yang was born in Hekou, Yunnan, China. She received the B.S. and M.S. degrees in electric engineering from Yunnan University, Kunming, China, in 2005 and 2007, respectively, and the Ph.D. degree from Kunming University of Science and Technology, Kunming, China, in 2010.

She is currently working at the School of Information Science and Engineering, Yunnan University. Her main research interests include wireless communication, computational electromagnetism, and electromagnetic theory.

Ming Huang was born in Wenshan, Yunnan, China. He received the B.S. and M.S. degrees in electric engineering from Yunnan University, Kunming, China, and the Ph.D. degree in microwave engineering from Kunming University of Science and Technology, Kunming, in 1984, 1987, and 2006, respectively.

He is currently a Professor at the School of Information Science and Engineering, Yunnan University. One of his research papers was highlighted by *Nature China* in June, 2007. His main research interests include wireless communication, microwave power application, and metamaterials. In his research area, he has (co-) authored 5 books, over 90 refereed journal papers, and international conference papers.

Jun Sun was born in Zhao Tong, Yunnan, China. He received the B.S. and M.S. degrees in electric engineering from Yunnan University, Kunming, China, in 2007 and 2009, respectively. Currently, he is working towards the Ph.D. degree at Kunming University of Science and Technology, Kunming.

His main research interests include computational electromagnetism and electromagnetic theory.